Available online at www.sciencedirect.com
SCIENCE DIRECT
Journal of Catalysis 226 (2004) 247–259
JOURNAL OF CATALYSIS
www.elsevier.com/locate/jcat

# Partial oxidation of methane to $H_2$ and CO over $Rh/SiO_2$ and $Ru/SiO_2$ catalysts

Q.G. Yan [a,*], T.H. Wu [b], W.Z. Weng [b,c], H. Toghiani [a], R.K. Toghiani [a], H.L. Wan [b,c,*], C.U. Pittman Jr. [d,*]

[a] *Center for Advanced Vehicular Systems and Dave C. Swalm School of Chemical Engineering, Box 5405, Mississippi State University, Starkville, MS 39762, USA*
[b] *Institute of Physical Chemistry, Zhejiang Normal University, Zhejiang 321004, People's Republic of China*
[c] *Department of Chemistry and the State Key Laboratory for Physical Chemistry of Solid Surface, Xiamen University, Xiamen, Fujian 361005, PR China*
[d] *Department of Chemistry, Box 9573, Mississippi State University, Starkville, MS 39762, USA*

Received 25 March 2004; revised 17 May 2004; accepted 22 May 2004

Available online 2 July 2004

**Abstract**

Partial oxidation of methane to syngas (POM) over $Rh/SiO_2$ and $Ru/SiO_2$ catalysts was investigated at 450–800 °C. Methane conversion and selectivity to both $H_2$ and CO were higher over $Rh/SiO_2$ than over $Ru/SiO_2$. The CO and $H_2$ selectivities substantially decreased with increasing GHSV over $Ru/SiO_2$ at 500 °C, while these selectivities remained nearly constant over $Rh/SiO_2$. Both the $CH_4$ conversions and the CO and $H_2$ selectivities increased slightly over $Rh/SiO_2$ at 700 °C as GHSV increases, while the $CH_4$ conversions and the CO and $H_2$ selectivities decreased slightly over $Ru/SiO_2$. Pulse reactions, transient reactions, and in situ microprobe Raman techniques were employed to investigate the oxidation of methane over $Rh/SiO_2$ and $Ru/SiO_2$ catalysts. CO was the main product when $Rh/SiO_2$ was exposed to methane pulsing at 700 °C. No $CO_2$ was detected during the first pulse over the $Rh/SiO_2$ catalysts. However, $CO_2$ was formed in every pulse over $Ru/SiO_2$. Transient results showed that CO was formed prior to $CO_2$ generation over $Rh/SiO_2$ catalysts. $CO_2$ was the primary product over $Ru/SiO_2$ catalysts. In situ microprobe Raman spectroscopy at 450–600 °C demonstrated that $Ru/SiO_2$ surfaces contained significantly larger amounts of metal oxide species than $Rh/SiO_2$ during the POM reaction. The mechanisms of POM over the two catalysts are different. A direct oxidation process mainly occurs over the $Rh/SiO_2$ catalyst, while the dominant pathway over the $Ru/SiO_2$ catalyst is the indirect oxidation process.


*Keywords:* Partial oxidation; Methane; Syngas; $Rh/SiO_2$; $Ru/SiO_2$; Pulse reactions; Transient reaction; In situ microprobe Raman spectroscopy

## 1. Introduction

The greenhouse effect and the limited reserves of fossil fuels have encouraged studies of $CO_2$-neutral and renewable energy sources. One alternative energy source is hydrogen, which can be used to generate both electricity and heat in high efficiency fuel cells. Hydrogen is targeted as the next generation fuel since it produces water instead of $CO_2$. Fuel cell technology and high-pressure hydrogen tank storage are already in advanced development stages [1–4]. Several techniques are available for hydrogen production from hydrocarbons including steam reforming which is generally accompanied by a water gas-shift conversion and a hydrogen purification process. Steam reforming [SR, Eq. (1)] has constituted the dominant commercial process employed to produce synthesis gas from methane over the past several decades [5]:

$$CH_4 + H_2O \rightarrow CO + 3H_2, \qquad \Delta H_{298} = 206\ \text{kJ/mol}. \quad (1)$$

However, this process requires a large energy input and very complex processing. Therefore, to obtain hydrogen at a lower energy input, the partial oxidation of methane [POM, Eq. (2)] to hydrogen and carbon monoxide which was first studied by Prettre et al. [6] has been studied intensively in

* Corresponding authors.
*E-mail addresses:* yan@cavs.msstate.edu (Q.G. Yan), hlwan@xmu.edu.cn (H.L. Wan).

0021-9517/$ – see front matter 
doi:10.1016/j.jcat.2004.05.028

the past decade [7–22]:

$$CH_4 + 1/2O_2 \rightarrow CO + 2H_2, \qquad \Delta H_{298} = -35.7\ \text{kJ/mol}. \tag{2}$$

Partial oxidation of methane (POM) to syngas is slightly exothermic and more energy efficient than steam reforming of $CH_4$. A smaller reactor can be used to achieve high $CH_4$ conversion and selectivity to $H_2$ with short contact times ($\sim 10^{-3}$ s) [23]. Furthermore, POM is mechanically simpler than the steam reforming, since it is completed in a single reactor, without external heating. However, several problems must be solved before POM can be developed on the industrial scale. These include the cofeeding of $CH_4/O_2$ under explosive conditions [11], and the formation of local hot spots within catalyst beds that can irreversibly damage both the catalyst and the reactor [11,12]. Carbon deposition may deactivate the catalysts [13,14]. Therefore, understanding the reaction mechanism and the nature of the active catalytic sites is important. Despite many past studies of the partial oxidation of methane to syngas, engineering problems (heat and mass-transfer control) must still be solved and catalysts must be improved [14]. Thus, a better understanding of mechanisms and microkinetics is required [15].

Two major POM reaction mechanisms have been proposed. One involves total oxidation of a portion of the $CH_4$ followed by reforming the unconverted $CH_4$ with $CO_2$ and $H_2O$ to produce CO and $H_2$. This was proposed by Prettre et al. [6]. The other scheme, proposed by Schmidt et al. [17,18], postulates direct partial oxidation of $CH_4$ to CO and $H_2$ without the production of $CO_2$ and $H_2O$. Schmidt et al. also found that the POM reaction process is mass-transfer limited [19–22] and examined the role of boundary layer mass transfer on the selectivity during partial oxidation of $CH_4$ oxidation to CO and $H_2$ over Pt–Rh gauzes and Pt-coated ceramic monoliths [19,20]. This selectivity is strongly affected by the gas-flow rate and the catalyst geometry. Schmidt et al. concluded that mass transfer across the boundary layer over a catalyst surface strongly influences reactor selectivity for fast reactions. Several variables during $H_2$ and CO production were examined. Selectivity was improved by operating at higher gas and catalyst temperatures by maintaining high rates of mass transfer through the surface boundary layer and by using catalysts with high metal loadings. High flow rates minimized mass-transfer limitations, causing gauze, foam monoliths, and extruded monoliths to give similar selectivities and conversions. However, important differences resulted from different catalyst geometries and thermal conductivities.

Supported noble metal catalysts are mainly used for the POM reaction, including Rh, Ru, Pd, and Pt [24–27], and supported Ni catalysts [28–30]. The type of catalyst employed may strongly influence the reaction steps of catalytic POM. Elmasides and Verykios [31] investigated the partial oxidation of methane to synthesis gas over $Ru/TiO_2$ employing non-steady-state and steady-state isotopic transient experiments, combined with in situ DRIFT spectroscopy. Gas-phase $CH_4$ interacts with the catalyst surface, producing $CH_x$ surface species. Elmasides and Verykios determined that CO is the primary product, resulting from a surface reaction between carbon and adsorbed atomic oxygen on metallic Ru sites, while $CO_2$ derives from CO oxidation on oxidized Ru sites [31]. Mallens et al. [32,33] found differences using Rh versus Pt catalysts, in the selectivity toward CO and $H_2$ during POM. These differences were attributed to the lower activation energy for methane decomposition on Rh versus that on Pt. Mallens et al. suggested that the catalyst's ability to activate methane determines (1) the product distribution and (2) the concentration of active surface species of oxygen, carbon, and hydrogen. Fathi et al. [34] studied the partial oxidation of methane to syngas over platinum catalysts and proposed that the product distribution is determined by both the concentrations and the types of surface oxygen species present at the catalyst surface. Qin et al. [35] suggested that the support might also influence the concentration of adsorbed oxygen and, as a consequence, the activation of methane and the product distribution. Li et al. [36] studied the effect of gas-phase $O_2$, reversibly adsorbed oxygen, and oxidation state of the nickel in the $Ni/Al_2O_3$ catalyst on $CH_4$ decomposition and partial oxidation using transient response techniques at 700 °C. They concluded that the surface state of the catalyst affects the reaction mechanism and plays an important role in POM conversions and selectivities. Li et al. [36] also argued that direct oxidation is the major POM route, and that the indirect oxidation mechanism cannot become dominant under their experimental conditions.

The reaction steps in $CH_4$ oxidation to CO and $H_2$ over a Rh(1 wt%)/$\gamma$-$Al_2O_3$ catalyst were studied using in situ DRIFTS at 973 K by Buyevskaya et al. [37,38]. The product distribution and the resulting absorption band intensities of the adsorbates were strongly influenced by oxygen coverage and carbon deposits on the surface. $CH_4$ was dehydrogenated to deposited carbon and $H_2$, while simultaneously being oxidized to $CO_2$ and $H_2O$. Surface OH groups in the support were involved in the $CH_x$ conversion to CO via reforming reactions. These authors assumed that surface carbon reacted with $CO_2$ to contribute to CO formation. Weng et al. [39,40] employed in situ TR-FTIR to investigate partial methane oxidation to syngas over supported Rh and Ru catalysts at 500 °C. Their TR-FTIR spectra indicated that a significant difference in POM mechanisms occurred when employing supported Ru versus supported Ru catalysts. CO was the primary POM product over hydrogen-reduced and working-state Rh catalysts according to these TR-FTIR observations. In contrast, $CO_2$ was the primary POM product over supported Ru catalysts. Therefore, the direct oxidation of $CH_4$ was proposed as the main pathway with $Rh/SiO_2$, while the reforming of unreacted $CH_4$ to syngas dominated using $Ru/SiO_2$ and was accompanied by oxidation of a portion of the $CH_4$ to $CO_2$ and $H_2O$.

The present investigation concerns the partial oxidation of methane to syngas over $Rh/SiO_2$ and $Ru/SiO_2$ catalysts.

Interaction of $CH_4$/Ar or $CH_4/O_2$/Ar with both $Rh/SiO_2$ and $Ru/SiO_2$ catalysts was examined by pulse and transient reaction techniques with on-line mass spectrometry monitoring. In situ microprobe Raman spectroscopy was used to study the oxidation state of the catalyst's surface under POM reaction conditions. The catalysts were characterized by TPR, XRD, and $H_2$ chemisorption. The different results observed over $Rh/SiO_2$ versus those using $Ru/SiO_2$ are explained.

## 2. Experimental

### 2.1. Catalyst preparation

The supported Rh and Ru catalysts were prepared by solution impregnation. The support $SiO_2$ (Aldrich Chemical Company, 60–80 mesh, 406 $m^2/g$) was first impregnated with either a $RhCl_3 \cdot 3H_2O$ or a $RuCl_3 \cdot 3H_2O$ aqueous solution. The water was evaporated and the solids were dried overnight in a vacuum oven at 110 °C and calcined in air at 500 °C for 6 h. A series of 1.0, 2.0, and 4.0 wt% catalysts were prepared. No chlorine content was detected in either of the catalysts by XPS.

### 2.2. Catalytic performance tests

Catalytic reaction tests were carried out in a fixed-bed quartz microreactor (200 mm, 6 mm i.d.). A 250-mg catalyst sample was charged. The reaction system was first purged with nitrogen, and the catalyst was reduced under pure hydrogen flow (10 ml/min) at 500 °C for 0.5 h. Then, a mixed $CH_4/O_2$ gas stream was introduced. The ratio of $CH_4/O_2$ in the feed gas was held constant at 2.0 (molar ratio). Activity testing was carried out at a GHSV of $1 \times 10^5$, $1.5 \times 10^5$, and $2 \times 10^5$ $h^{-1}$, 450–800 °C and 1 atm. Analyses of the reactant/product mixtures were conducted on a Model 103G gas chromatograph with a TC detector. A carbon sieve TDX-01 column was used to separate $H_2$, CO, $O_2$, $CH_4$, and $CO_2$ using argon as the carrier gas. The column was maintained at 110 °C under an argon flow of 30 ml/min. The amount of carbon deposited on the catalysts after POM was obtained via combustion chromatography as previously described [13].

### 2.3. Temperature-programmed reduction (TPR), temperature-programmed desorption (TPD), pulsed reactions, and transient responses to step changes of the feed gases

TPR, TPD, pulsed reactions, and the transient responses to step changes in the feed gases were each carried out in a fixed-bed tubular quartz microreactor with an inner diameter of 3 mm and 18 cm length. A 50-mg catalyst sample was used in every run. An on-line Balzers quadruple mass spectrometer (QMS200) continuously monitored the effluent from the reactor. The effluents could contain $H_2$ ($m/z = 2$), He ($m/z = 4$), $CH_4$ ($m/z = 16$), $H_2O$ ($m/z = 18$), CO or $N_2$ ($m/z = 28$), $O_2$ ($m/z = 32$), and $CO_2$ ($m/z = 44$).

#### 2.3.1. TPR experiments

Fresh catalyst was first pretreated in a He flow at 500 °C for 1 h. The sample was then cooled to room temperature and the He flow was switched to a 3% by volume $H_2$ in $N_2$ flow. After the effluent concentrations had reached constant values for 30 min, the temperature was ramped at a rate of 15 °C/min to 1000 °C.

#### 2.3.2. $O_2$-TPD experiments

The catalyst was first pretreated at 700 °C under flowing pure oxygen for 10 min and then cooled to room temperature. Then a He flow was introduced for 30 min. The temperature was next increased at a rate of 20 °C/min to 1000 °C while helium was next passed through the catalyst bed.

The pulse reaction experiments were performed at 700 °C and 1 atm. Helium (30 ml/min) was used as the carrier gas, and 1 ml $CH_4$/Ar (1/10) per pulse was employed. The sample was continuously exposed to a flow of 30 ml/min He. The desired gas was pulsed into this He stream. The reaction products were quantified with a mass spectrometer.

The transient experiments were performed at 500 and 700 °C under 1 atm. The reactants were $CH_4/O_2$/Ar (2/1/20).

### 2.4. In situ microprobe Raman characterization

In situ microprobe Raman catalyst characterization experiments were performed using a home-built high-temperature in situ microprobe Raman cell, allowing Raman spectra of the catalysts to be obtained from room temperature to 700 °C under different gas atmospheres. Raman spectra were recorded on a Dilor LabRam I cofocal microprobe Raman system. The exciting wavelength of 514.5 nm was generated with an $Ar^+$ laser with a power of 15 mW and a spot size of ca. 3 $\mu m^2$. The laser beam was focused on the top of the catalyst bed. In each experiment, the catalyst (ca. $2.5 \times 10^{-3}$ ml) was first subjected to a flow of $O_2$ (99.995%) at 500 °C for 30 min. After $O_2$ pretreatment, the Raman spectra of the catalysts were obtained. Then the treatment was switched to a $H_2$/Ar (5/95, molar ratio) flow at 500 or 600 °C for 5 min and the Raman spectra of $H_2$-reduced sample were obtained. Finally, the $H_2$-reduced catalyst bed was subjected to a flow of $CH_4/O_2$/Ar (2/1/45, molar ratio) at 500 or 600 °C for 5 min, and then the Raman spectra of the catalysts were obtained under POM conditions at a flow rate of 5 ml/min. All the Raman spectra were recorded under steady-state conditions.

### 2.5. X-ray diffraction (XRD) and metal dispersions

XRD patterns were obtained with a Philips PW 1840 powder diffractometer. Co-K$\alpha$ radiation was employed, covering $2\theta$ between 20 and 80°. Metal dispersions on the catalysts were measured by $H_2$ chemisorption at room temperature. The percentage dispersion of Rh or Ru metal was calcu-

lated assuming a H/M atomic ratio of 1 [41]. The metal dispersion was estimated by hydrogen chemisorption at room temperature. The catalyst sample was first reduced under hydrogen at 500 °C for 1 h, evacuated at 500 °C under high vacuum for 30 min, and then cooled to room temperature under vacuum for chemisorption.

## 3. Results

### 3.1. Catalytic performance

A $CH_4/O_2$ gas mixture with a molar ratio of 2/1 was used as the feed gas, in POM reactions conducted between 450 and 800 °C at 1 atm, and at a GHSV of 150,000 $h^{-1}$ over 1 wt% $Rh/SiO_2$ and 1 wt% $Ru/SiO_2$. The effect of temperature on catalyst reactivity was investigated. Product distributions, conversions, and selectivities are presented in Table 1.

The conversion of methane and selectivity to syngas both increased with increasing temperature. The conversions and selectivities were high at high temperatures ($\geqslant$ 700 °C) for both catalysts. But, conversion of $CH_4$ and $O_2$ and selectivity of CO and $H_2$ are obviously different for these two catalysts at low temperatures (450–600 °C). Specifically, the conversion of $CH_4$ and selectivity to both $H_2$ and CO over $Rh/SiO_2$ catalyst were higher than those over $Ru/SiO_2$. The $O_2$ conversion was a little lower over $Rh/SiO_2$ than that over $Ru/SiO_2$. After completing the POM reactions, combustion chromatography was employed to detect any carbon deposition on the catalysts. However, no evidence for carbon deposition was detected for either catalyst after the POM reaction.

Table 2 shows the effect of space velocity on the $CH_4$ and oxygen conversions and on syngas selectivities at both 500 and 700 °C. At 500 °C, the $CH_4$ conversion and the CO and $H_2$ selectivities decreased with increasing space velocity over 1 wt% $Ru/SiO_2$, while on 1.0 wt% $Rh/SiO_2$ the $CH_4$ conversion and the CO and $H_2$ selectivities maintained nearly constant. Both the $CH_4$ conversions and the CO and $H_2$ selectivities increased slightly over $Rh/SiO_2$ at 700 °C as GHSV increases, while the $CH_4$ conversions and the CO and $H_2$ selectivities decreased slightly over $Ru/SiO_2$.

### 3.2. X-ray diffraction, temperature-programmed reduction ($H_2$-TPR), and metal dispersions on catalysts

#### 3.2.1. Catalyst XRD patterns

The XRD patterns of 2.0 wt% Rh(O)/$SiO_2$ and 2.0 wt% Ru(O)/$SiO_2$ are shown in Fig. 1. The use of (O) indicates these catalysts had been calcined in the presence of oxygen. X-ray diffraction analysis showed that a mixture of $Rh_2O_3$ and $SiO_2$ phases was obtained for the 2.0% Rh(O)/$SiO_2$ catalyst after calcinations. $RuO_2$ and $SiO_2$ phases were found on the 2.0 wt% Ru(O)/$SiO_2$ catalyst. The 1.0 wt% Rh(O)/$SiO_2$ catalyst was analyzed by XRD (not shown here), but no diffractions corresponding to Rh or $Rh_2O_3$ were present. Only $SiO_2$ was detected in Rh(O)/$SiO_2$. Thus, rhodium particles must be highly dispersed with sizes smaller than the detection limit of the instrument. One of the reasons for this high dispersion is that the rhodium content is very low. XRD of 1.0 wt% Ru(O)/$SiO_2$ exhibited the $SiO_2$ phase with very weak $RuO_2$ lines. The XRD described here was performed on 2.0 wt% metal catalysts.

#### 3.2.2. TPR of catalysts

TPR experiments were conducted from 25 to 500 °C to investigate the reducibility of rhodium oxide and ruthenium oxide on the 1.0% Rh(O)/$SiO_2$ and 1% Ru(O)/$SiO_2$ catalysts. Fig. 2 illustrates hydrogen consumption by these

Table 1
Methane and oxygen conversion and the selectivity to $H_2$ and CO during the partial oxidation of methane over 1.0 wt% $Rh/SiO_2$ and 1.0 wt% $Ru/SiO_2$ catalysts[a]

| Catalyst | Temperature (°C) | Outlet gas composition (%) | | | | | Conversion (%) | | Selectivity (%) | |
|---|---|---|---|---|---|---|---|---|---|---|
| | | $H_2$ | $O_2$ | $CH_4$ | CO | $CO_2$ | $CH_4$ | $O_2$ | $H_2$ | CO |
| 1.0 wt% $Rh/SiO_2$ | 450 | 28.0 | 8.3 | 36.5 | 12.0 | 15.2 | 42.7 | 80.5 | 51.5 | 44.1 |
| | 500 | 46.1 | 3.5 | 16.5 | 19.8 | 14.1 | 67.2 | 90.8 | 68.2 | 58.4 |
| | 550 | 52.1 | 1.2 | 10.5 | 25.9 | 10.2 | 77.5 | 96.5 | 72.2 | 77.5 |
| | 600 | 57.2 | 0.5 | 5.9 | 29.6 | 6.8 | 86.0 | 98.0 | 78.8 | 81.3 |
| | 650 | 61.0 | 0 | 3.7 | 30.8 | 4.5 | 90.5 | 100 | 86.4 | 87.3 |
| | 700 | 64.0 | 0 | 1.9 | 32.6 | 1.5 | 94.7 | 100 | 93.8 | 95.6 |
| | 750 | 64.9 | 0 | 1.2 | 32.8 | 1.1 | 96.6 | 100 | 95.7 | 96.7 |
| | 800 | 65.7 | 0 | 0.8 | 33.0 | 0.5 | 97.6 | 100 | 98.0 | 98.5 |
| 1.0 wt% $Ru/SiO_2$ | 450 | 25.9 | 6.0 | 39.8 | 9.0 | 19.3 | 39.8 | 88.3 | 45.7 | 31.8 |
| | 500 | 43.0 | 1.6 | 19.8 | 18.4 | 17.2 | 64.2 | 93.5 | 60.4 | 51.7 |
| | 550 | 50.5 | 0.7 | 13.0 | 23.1 | 12.7 | 73.1 | 97.8 | 70.8 | 65.4 |
| | 600 | 54.7 | 0 | 8.9 | 25.9 | 9.4 | 83.7 | 100 | 76.4 | 78.5 |
| | 650 | 60.5 | 0 | 4.2 | 30.1 | 5.2 | 89.4 | 100 | 85.7 | 85.3 |
| | 700 | 63.6 | 0 | 2.0 | 32.6 | 1.8 | 94.3 | 100 | 92.4 | 94.8 |
| | 750 | 64.7 | 0 | 1.1 | 32.9 | 1.3 | 96.9 | 100 | 94.6 | 95.6 |
| | 800 | 65.5 | 0 | 0.9 | 32.7 | 0.9 | 97.4 | 100 | 97.8 | 97.0 |

[a] Reaction conditions: pressure = 1 atm, $CH_4/O_2$ = 2/1, GHSV = 150,000 $h^{-1}$.

Table 2
Effect of gas hourly space velocity (GHSV) on methane conversion and the selectivity to $H_2$ and CO during the partial oxidation of methane over 1.0 wt% $Rh/SiO_2$ and 1.0 wt% $Ru/SiO_2$ catalysts[a]

| Catalyst | Temperature (°C) | GHSV ($h^{-1}$) | $CH_4$ conversion (%) | | Selectivity (%) | |
|---|---|---|---|---|---|---|
| | | | $CH_4$ | $O_2$ | $H_2$ | CO |
| 1.0 wt% $Rh/SiO_2$ | 500 | 100,000 | 68.8 | 91.7 | 69.5 | 59.1 |
| | 500 | 150,000 | 67.2 | 90.8 | 68.2 | 58.4 |
| | 500 | 200,000 | 67.0 | 90.0 | 66.2 | 56.5 |
| | 700 | 100,000 | 93.5 | 100 | 93.4 | 95.3 |
| | 700 | 150,000 | 94.7 | 100 | 93.8 | 95.6 |
| | 700 | 200,000 | 94.6 | 100 | 94.7 | 96.7 |
| 1.0 wt% $Ru/SiO_2$ | 500 | 100,000 | 66.3 | 95.1 | 66.5 | 57.9 |
| | 500 | 150,000 | 64.2 | 93.5 | 60.4 | 51.7 |
| | 500 | 200,000 | 61.1 | 91.0 | 53.6 | 45.4 |
| | 700 | 100,000 | 94.5 | 100 | 91.7 | 95.3 |
| | 700 | 150,000 | 94.3 | 100 | 92.4 | 94.8 |
| | 700 | 200,000 | 93.9 | 100 | 91.6 | 94.6 |

[a] Reaction conditions: pressure = 1 atm, $CH_4/O_2 = 2/1$.

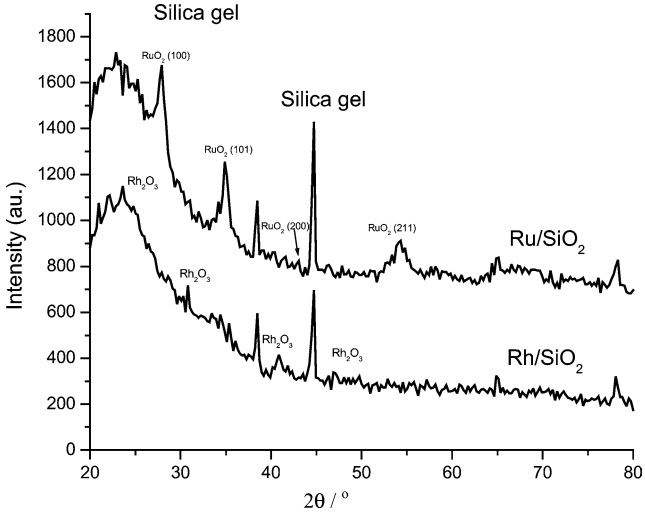


Fig. 1. XRD patterns of $Rh/SiO_2$ and $Ru/SiO_2$ catalysts.

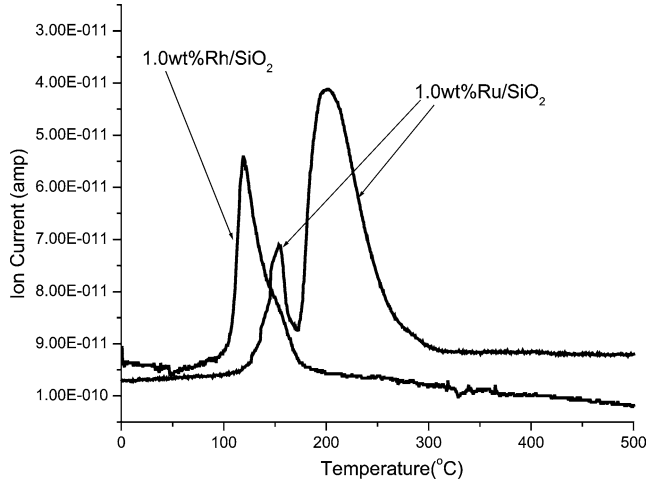


Fig. 2. Temperature-programmed reduction (TPR) profiles of the 1 wt% $Rh/SiO_2$ catalyst and the 1 wt% $Ru/SiO_2$ catalyst.

catalysts as a function of the temperature during the reduction. Reduction of the 1.0% $Rh(O)/SiO_2$ catalyst took place between 80 and 180 °C and was characterized by one sharp peak with a maximum temperature around 120 °C. The hydrogen consumption corresponds to a full reduction of rhodium oxide to $Rh^0$, i.e., ($Rh_2O_3 + 3H_2 \rightarrow 2Rh + 3H_2O$). The reduction profile for 1.0 wt% $Ru(O)/SiO_2$ exhibited peaks different from those for 1.0% $Rh(O)/SiO_2$. Two reduction peaks were found in reductions of 1.0% $Ru(O)/SiO_2$ between 80 and 250 °C. These two peaks had $T_{max} =$ 150 °C and $T_{max} = 200$ °C, with the latter accounting for significantly more hydrogen uptake. The lower temperature (150 °C) TPR peak has been assigned to the reduction of well-dispersed $RuO_x$ species [42], and the high-temperature peak is attributed to the reduction of $RuO_2$ particles ($RuO_2 + 2H_2 \rightarrow Ru + 2H_2O$) [43]. The hydrogen consumption for 1.0% $Ru(O)/SiO_2$, calculated from the area of the reduction peak, was about three times that of 1.0% $Rh(O)/SiO_2$. About $4.9 \times 10^{-6}$ mol Rh or Ru atoms are present in 50-mg samples of these catalysts. Thus, the 1.0 wt% $Rh(O)/SiO_2$ catalyst must consume $7.29 \times 10^{-6}$ mol $H_2$ in TPR reactions if all the rhodium were present as $Rh_2O_3$ and all $Rh_2O_3$ is completely reduced to $Rh^0$ and $H_2O$. Similarly, 1.0 wt% $Ru(O)/SiO_2$ should consume $9.9 \times 10^{-6}$ mol $H_2$ if all $RuO_2$ were reduced.

### 3.2.3. Metal dispersions

The metal dispersion of the reduced catalysts was obtained by $H_2$ chemisorption at 298 K. The percentage dispersion of Rh or Ru metal, calculated assuming a H/M atomic ratio of 1, is shown in Table 3. The dispersion of rhodium was 95% for 1.0 wt% $Rh/SiO_2$ and ruthenium dispersion was 33% for 1.0 wt% $Ru/SiO_2$. The dispersion of $Ru/SiO_2$ is much less than that of $Rh/SiO_2$. The dispersions for both the 2% Rh and 2% Ru catalysts were about half of those found in the 1% Rh and Ru catalysts, respectively.

Table 3
The metal dispersion of the catalysts

| Catalyst | H/M (atomic ratio) | Dispersion (%) |
|---|---|---|
| 1.0 wt% $Rh/SiO_2$ | 0.95 | 95 |
| 2.0 wt% $Rh/SiO_2$ | 0.50 | 50 |
| 1.0 wt% $Ru/SiO_2$ | 0.33 | 33 |
| 2.0 wt% $Ru/SiO_2$ | 0.15 | 15 |

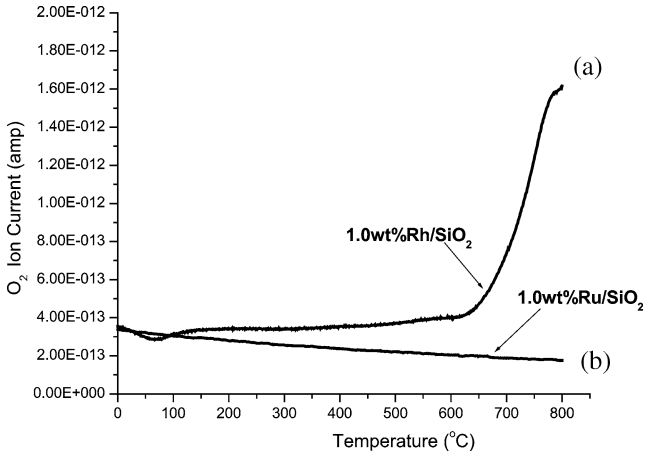


Fig. 3. $O_2$-TPD profile of (a) the 1 wt% $Rh/SiO_2$ catalyst and (b) the 1 wt% $Ru/SiO_2$ catalyst.

### 3.3. Temperature-programmed desorption of $O_2$ ($O_2$-TPD)

$O_2$-TPD experiments were carried out to characterize the metal oxides in $Rh(O)/SiO_2$ and $Ru(O)/SiO_2$. Both catalysts were oxidized under a pure oxygen flow (10 ml/min) at 700 °C for 30 min and then cooled to room temperature before the TPD experiments were conducted. $O_2$-TPD of the two catalysts is depicted in Fig. 3. $O_2$ started to desorb from the 1.0 wt% $Rh(O)/SiO_2$ catalyst around 550 °C and the desorption peak maximum was reached at ca. 800 °C, where the reaction $2Rh_2O_3 \rightarrow 4Rh + 3O_2$ may occur. No oxygen desorption peak occurred during $O_2$-TPD of 1 wt% $Ru(O)/SiO_2$, perhaps because the reaction $3RuO_2 \rightarrow Ru + 2RuO_3$ (or $RuO_4$) takes place instead at high temperatures [44].

### 3.4. Interaction of methane with the catalysts by pulsed reactions

Oxygen-free $CH_4$ pulsing reactions were carried out over both 1.0 wt% $Rh/SiO_2$ and 1.0 wt% $Ru/SiO_2$ at 700 °C and 1 atm pressure. The CO and $CO_2$ produced are shown in Fig. 4. Fig. 4a depicts the CO and $CO_2$ formation responses during $CH_4$ pulsing over unreduced $Rh(O)/SiO_2$. Large amounts of CO and $CO_2$ were observed at the first pulse. The formation of CO and $CO_2$ may result from $CH_4$ reacting with the active oxygen species on the Rh and/or $SiO_2$ support surface. However, no $CO_2$ formation was observed after the first pulse. The concentration of oxygen species on the catalyst surface might be too low after the first pulse to form $CO_2$. Readily observed tailing of the CO peak occurred after each $CH_4$ pulse. The CO tailed for 2–3 min before reaching background level, while $CO_2$ peaks lasted only 5–6 s. We suggest that adsorbed $CH_x$ ($x = 0$–3) reacts with oxygen species to form CO, while $CO_2$ might come from total oxidation methane ($3CH_4 + 4Rh_2O_3 \rightarrow 8Rh + 3CO_2 + 6H_2O$).

The production of $CO_2$ and CO in $CH_4$ pulses over reduced $Rh/SiO_2$ at 700 °C is shown in Fig. 4b. Similar to the response of oxidized $Rh(O)/SiO_2$, the intensities of CO and $CO_2$ are high during the first pulse reduced over $Rh/SiO_2$. $CO_2$ appears also only at the first pulse over the reduced $Rh/SiO_2$. No $CO_2$ is detected after the first pulse. The amount of CO produced was much lower than that formed with $Rh(O)/SiO_2$. CO peaks tailed when produced by methane pulsing over both the oxidized $Rh(O)/SiO_2$ and the reduced $Rh/SiO_2$ catalysts.

$CH_4$ pulsing over the unreduced $Ru(O)/SiO_2$ also produces CO and $CO_2$ (Fig. 4c). Large amounts of CO and $CO_2$ were detected in the first pulse, and the intensity was much stronger than that found in the evolution of CO and $CO_2$ from the $Rh/SiO_2$ catalyst. However, unlike the $Rh/SiO_2$ catalyst, $CO_2$ is formed at every pulse over the $Ru(O)/SiO_2$ catalyst. Pulsing $CH_4$ over reduced $Ru/SiO_2$ also produced both CO and $CO_2$ with every pulse (Fig. 4d). The reaction ($2RuO_2 + CH_4 \rightarrow 2Ru + CO_2 + 2H_2O$) will take place over $Ru/SiO_2$. These products are very similar to those formed over the unreduced $Ru/SiO_2$, except that the intensities of the CO and $CO_2$ peaks are higher than those from reduced $Ru/SiO_2$. Tailing of the CO peak is also observed during pulsing over $Ru/SiO_2$ and the tailing time varies from 2 to 3 min. No $CO_2$ tailing occurs.

Pulse methane reactions were conducted over $Rh/SiO_2$ and $Ru/SiO_2$ catalysts without added oxygen (Fig. 4a–4d). Any methane oxidation in these experiments must be derived from oxygen originating from the solid catalyst systems. In each pulse experiment, 1 ml of reactants ($CH_4/Ar = 1/10$) was introduced. Each 1 ml contains about $4.46 \times 10^{-6}$ mol methane. If all the Rh is present as $Rh_2O_3$, the unreduced $Rh/SiO_2$ catalyst will consume ca. $1.82 \times 10^{-6}$ mol $CH_4$. Similarly, the unreduced $Ru/SiO_2$ should consume $2.50 \times 10^{-6}$ mol $CH_4$ if all the Ru is present as $RuO_2$. So a single $CH_4/Ar$ pulse of 1 ml would be sufficient to reduce all the rhodium and ruthenium oxides ($\sim$ 1.0 wt%, ca. $4.9 \times 10^{-6}$ mol) in each of these 50-mg catalyst samples to the metallic state.

### 3.5. Transient reactions of $CH_4/O_2/Ar$ with the catalysts

Transient experiments were performed at 500 and 700 °C under 1 atm using step changes in the feed gas from He to $CH_4/O_2/Ar$. The responses of the product distribution to these step changes, where oxygen has now been added, are shown in Fig. 5.

Fig. 5a plots the responses to a step change in the feed gas from helium to $CH_4/O_2/Ar$ over unreduced $Rh(O)/SiO_2$

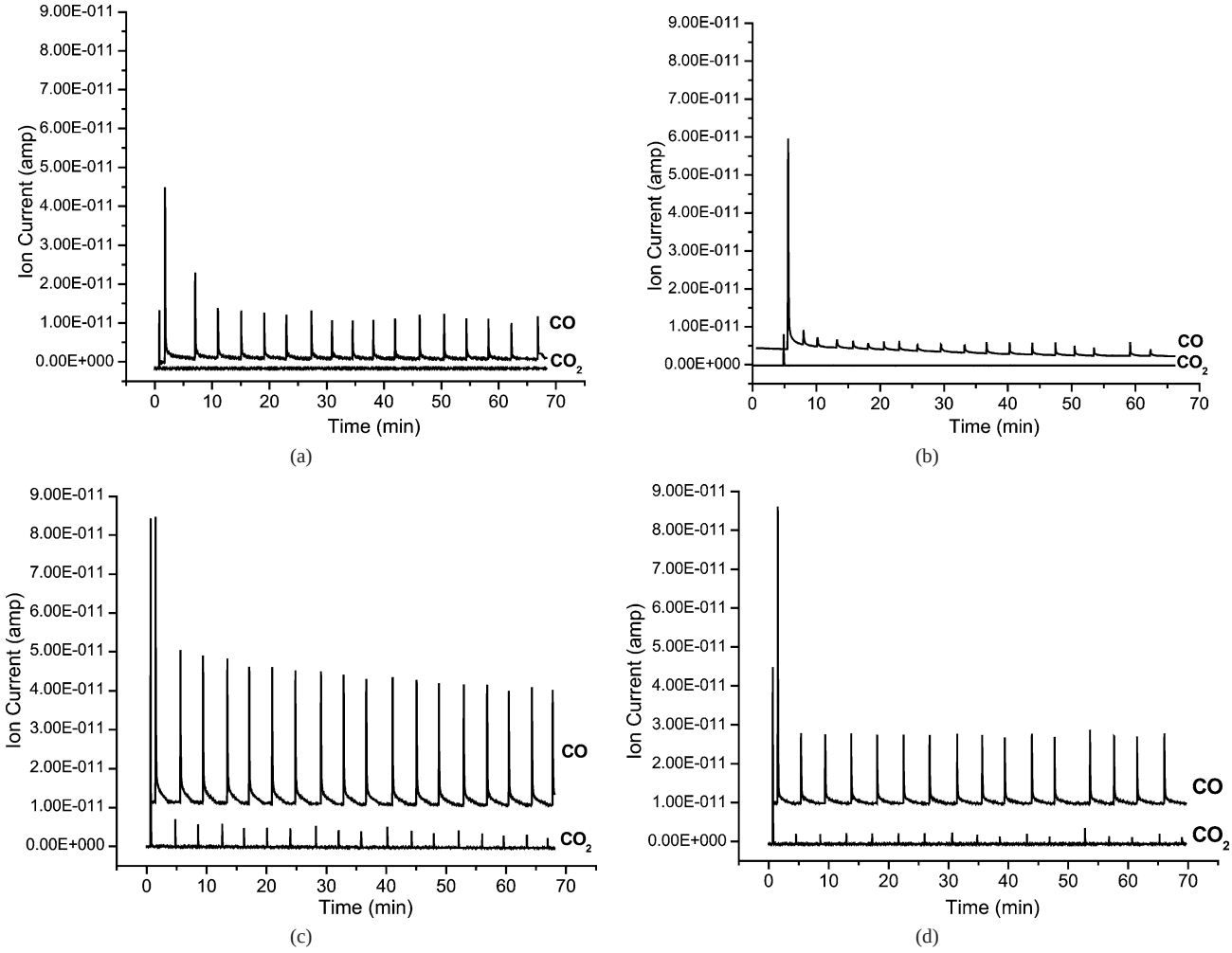


Fig. 4. CO and $CO_2$ produced by pulsing $CH_4$ at 700 °C over (a) the preoxidized Rh(O)/$SiO_2$, (b) the prereduced Rh/$SiO_2$, (c) the preoxidized Ru(O)/$SiO_2$, and (d) the prereduced Ru/$SiO_2$ catalyst.

at 500 °C. It is obvious that $CO_2$ (4.0 s) appears before CO (4.5 s).

Fig. 5b plots the products versus time as the step change from helium to $CH_4/O_2$/Ar was made at 500 °C over the reduced Rh/$SiO_2$. This Rh/$SiO_2$ catalyst had been previously subjected to a 30 min reduction by $H_2$ at 500 °C. CO and $CO_2$ appear at the same time (3.7 s) and then increase to a steady level after the gas feed switch.

Fig. 5c plots the product responses to changing the feed gas from helium to $CH_4/O_2$/Ar over oxidized Rh(O)/$SiO_2$ at 700 °C. CO (2.7 s) appears at once and sharply increases to a steady level. CO appears slightly before $CO_2$ (4.0 s). The amount of $CO_2$ increases to a steady state level but the quantity of $CO_2$ formed is much lower than the amount of $H_2$ and CO generated.

The responses of the step change in the feed gases from helium to $CH_4/O_2$/Ar were also obtained over the reduced Rh/$SiO_2$ catalyst (Fig. 5d) which had been previously subjected to a flow of $H_2$ for 30 min at 700 °C. CO (3.9 s) and $H_2$ appear immediately after the change from He to $CH_4/O_2$/Ar was made at 700 °C. The amounts of $H_2$ and CO increase sharply to reach their maximum and then decrease slowly to a constant level. Only a very tiny quantity of $CO_2$ was detected (5.0 s) after the step change.

The product responses to a feed gas change from He to $CH_4/O_2$/Ar over unreduced Ru(O)/$SiO_2$ at 500 °C are shown in Fig. 5e. $CO_2$ appeared at 2.6 s after this step change, while CO appeared at 3.0 s. Fig. 5f depicts the transient product response to the feed gas step change over the reduced Ru/$SiO_2$ catalyst at 500 °C. The $CO_2$ (3.3 s) appears prior to CO (4.5 s).

The product responses to a feed gas change from He to $CH_4/O_2$/Ar over unreduced Ru(O)/$SiO_2$ at 700 °C are shown in Fig. 5g. $CO_2$ (2.2 s) appears before CO (4.2 s) after the step change. This contrasts with the behavior induced by the oxidized Rh(O)/$SiO_2$ catalyst at 700 °C. Furthermore, $CO_2$ reaches a maximum first and then decreases rapidly to the background level. CO is rapidly formed, rising quickly followed by a long gradual further increase.

Fig. 5h depicts the transient product response to the He to $CH_4/O_2$/Ar step change over the reduced Ru/$SiO_2$ catalyst at 700 °C. $CO_2$ (3.0 s) still appears prior to CO (3.6 s); how-

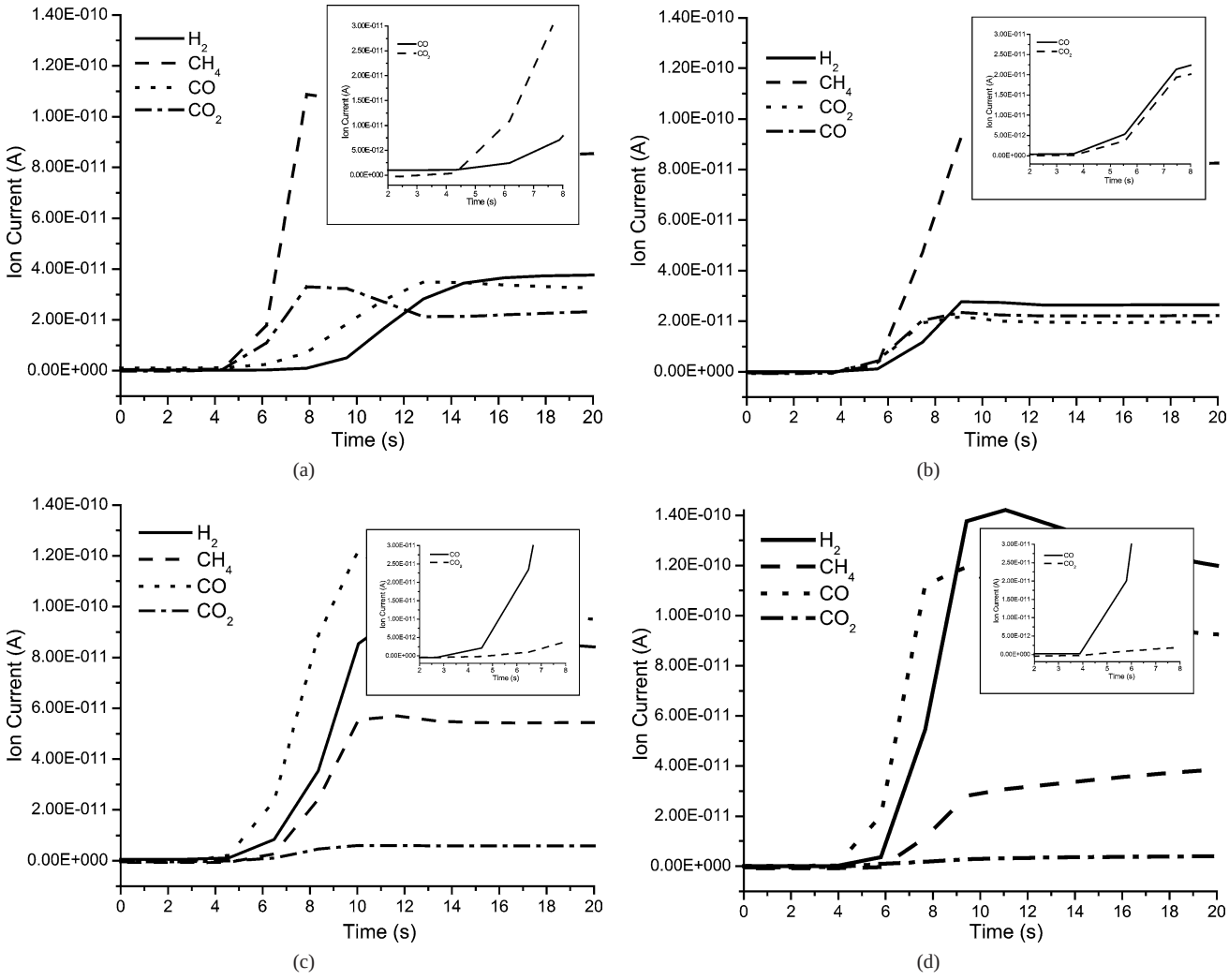


Fig. 5. Transient responses upon a step change in feed gas from He to $CH_4/O_2/Ar$ at 500 and 700 °C over (a) preoxidized $Rh/SiO_2$ at 500 °C, (b) prereduced $Rh(O)/SiO_2$ at 500 °C, (c) preoxidized $Rh/SiO_2$ at 700 °C, (d) prereduced $Rh(O)/SiO_2$ at 700 °C, (e) preoxidized $Ru(O)/SiO_2$ at 500 °C, (f) prereduced $Ru/SiO_2$ at 500 °C, (g) preoxidized $Ru(O)/SiO_2$ at 700 °C, and (h) prereduced $Ru/SiO_2$ at 700 °C.

ever, only very small quantities of $CO_2$ were found to form over reduced $Ru/SiO_2$ catalyst.

### 3.6. *In situ microprobe Raman spectroscopy*

The Raman spectrum of 4 wt% $Rh/SiO_2$ was recorded at 500 °C under an $O_2$ flow (Fig. 6a). A broad band centered at 491 $cm^{-1}$. It was attributed to $Rh_2O_3$ [42]. Many studies of Rh catalysts have proved that complete oxidation of Rh to $Rh_2O_3$ takes place under an $O_2$ atmosphere at temperatures above 500 °C [45]. The $Rh_2O_3$ band at 491 $cm^{-1}$ disappeared when the $O_2$-pretreated $Rh/SiO_2$ sample was reduced in a flow of $H_2/Ar$ at 500 °C. No $Rh_2O_3$ 491 $cm^{-1}$ band appeared when the $H_2/Ar$ pretreated $Rh/SiO_2$ was switched to a flow of $CH_4/O_2/Ar$ at the same temperature. Thus, surface oxides of rhodium do not form in observable quantities under POM conditions at 500 °C. At higher temperatures the thermal desorption of oxygen from rhodium surfaces was shown to become more pronounced (Section 3.3). Thus, metallic rhodium surfaces are available from 500 to 800 °C. The Raman spectrum of 4 wt% $Ru/SiO_2$ catalyst was recorded at 600 °C under $O_2$ (Fig. 6b). Two bands attributable to ruthenium oxide appear at 489 and 609 $cm^{-1}$ [46,47]. These bands vanished when the $O_2$-pretreated 4 wt% $Ru/SiO_2$ was subsequently placed under a flow of $H_2/Ar$ at 600 °C, and then these bands reappeared when a flow of $CH_4/O_2/Ar$ gases was introduced at the same temperature. Thus, oxides of ruthenium form on the catalyst under POM conditions at 600 °C.

## 4. Discussion

### 4.1. *Characterization of $Rh/SiO_2$ and $Ru/SiO_2$ catalysts and effects of oxidation states on POM mechanism over $Rh/SiO_2$ and $Ru/SiO_2$ catalysts*

$Rh_2O_3$ is the most stable oxide of rhodium [48]. Complete oxidation of Rh to $Rh_2O_3$ occurs above 500 °C un-

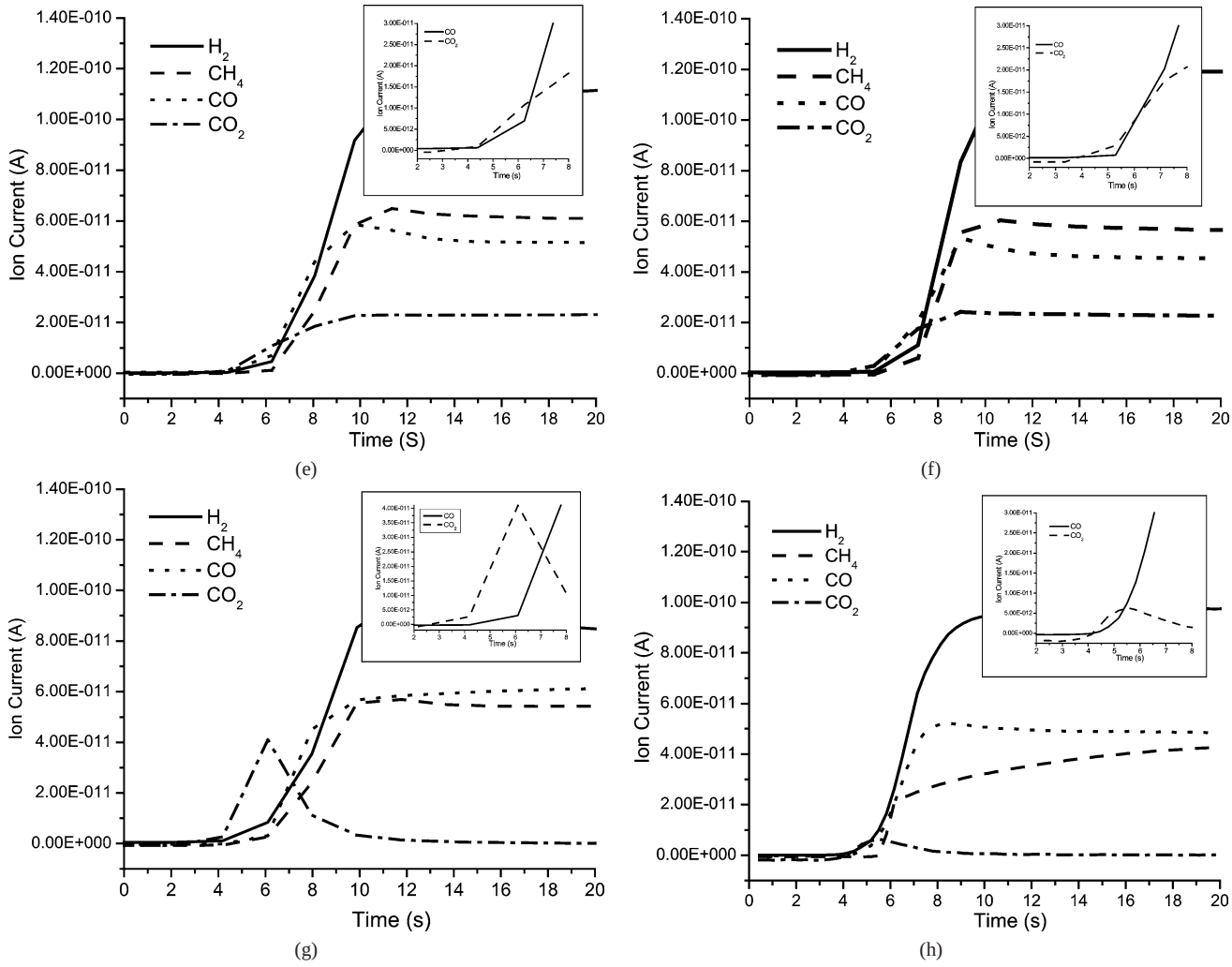


Fig. 5. Continued.

der an $O_2$ atmosphere. $Rh_2O_3$ thermally decomposes only at 1100 °C [49], but it easily reduces with hydrogen at 200 °C [50]. Facile reduction of Rh(O)/$SiO_2$ by $H_2$ was observed at 120 °C in TPR experiments (Fig. 2). Ruthenium oxides including $Ru_2O_3$, $RuO_2$, $RuO_3$, and $RuO_4$ are more resistant to reduction than $Rh_2O_3$ [51]. The reduction of 1 wt% Rh(O)/$SiO_2$ takes place between 80 and 180 °C with the $H_2$ uptake peak occurring at $T_{max} = 120$ °C (Fig. 2). In contrast, Ru(O)/$SiO_2$ exhibits two hydrogen uptake peaks, with the smaller peak maximizing at 150 °C and the larger at 200 °C. A single reduction peak from Rh(O)/$SiO_2$ is consistent with excellent surface dispersion of the rhodium oxides on $SiO_2$. The two peaks (150 and 200 °C) in the TPR profile of Ru(O)/$SiO_2$ suggest the presence of two different ruthenium oxides [42] where Ru–O bonding is stronger than rhodium–oxygen bonding. The 150 °C TPR peak has been assigned to the reduction of well-dispersed $RuO_x$ species [42], while the high-temperature peak is attributed to the reduction of $RuO_2$ particles ($RuO_2 + 2H_2 \rightarrow Ru + 2H_2O$) [43].

Different surface metal oxidation states and/or the relative bond strengths of transition metals with oxygen can result in different mechanisms [32,33,35]. Stronger M–O bond strengths give more stable transition metal oxides. This could lead to differences in activity and mechanism during POM.

$CH_4$ pulse experiments provide some mechanistic insight. A noticeable difference was observed in the reaction of pure methane over the unreduced versus the reduced 1.0 wt% Rh and Ru catalysts at 700 °C. CO is both the direct product and the major product over unreduced and reduced 1.0 wt% Rh/$SiO_2$. This result is in accord with previous in situ time-resolved FTIR spectroscopy studies [39,40], in which CO was the primary POM reaction product over both reduced Rh metal and working state Rh/$SiO_2$ catalysts. In contrast, $CO_2$ is a primary product during POM over Ru/$SiO_2$. $CO_2$ was formed in every pulse when oxygen-free $CH_4$ was pulsed over Ru/$SiO_2$ at 700 °C. Therefore, it is clear that the oxygen, contained in the ruthenium oxides, was responsible for both $CO_2$ and CO formation occurring over Ru/$SiO_2$. In contrast, $CO_2$ was only formed during the first

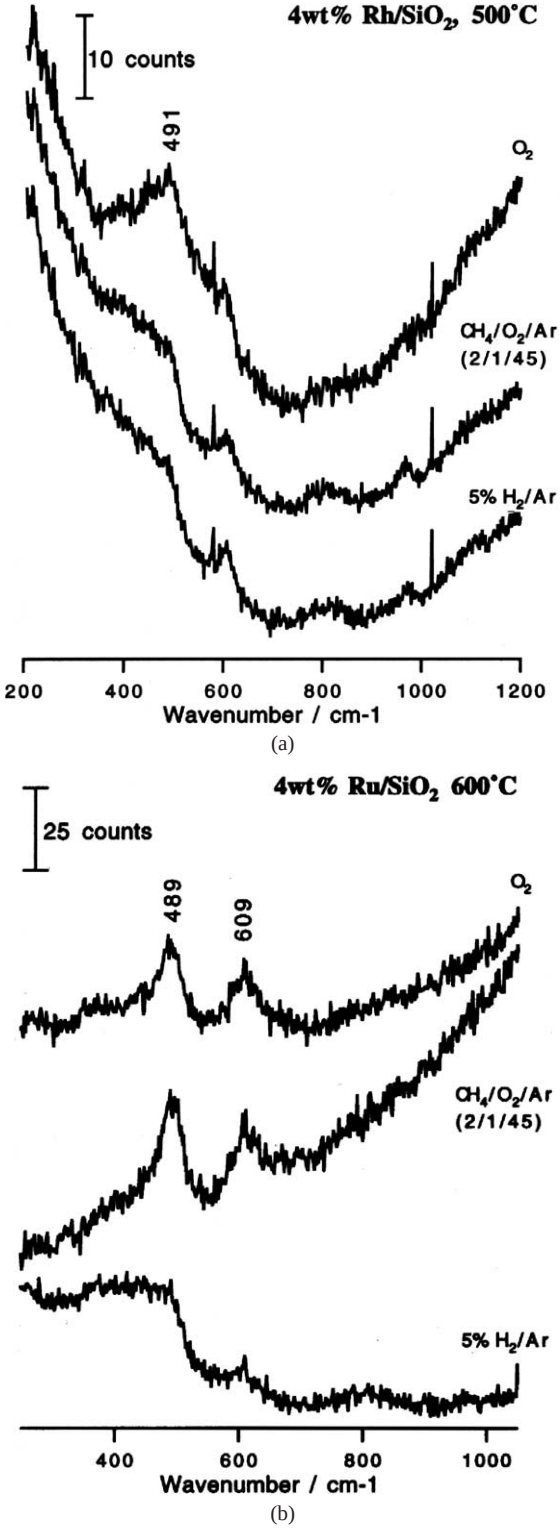


Fig. 6. In situ Raman spectra of (a) 4 wt% $Rh/SiO_2$ at 500 °C and (b) 4 wt% $Ru/SiO_2$ at 600 °C when each of these catalysts was under $O_2$, $CH_4/O_2/Ar$ (2/1/45), or 5% $H_2$/95% Ar.

pulse and never thereafter when methane was pulsed over $Rh/SiO_2$. Thus, surface oxygen on rhodium sites favors the formation of CO. Apparently, the very small rhodium oxide surface concentration is too low to continue to fully oxidize $CH_x$ species on the rhodium catalyst's surface to $CO_2$ before CO desorbs. Thus, the amount and state of the metal oxides present on the $Rh/SiO_2$ and $Ru/SiO_2$ catalysts are of seminal importance to the methane activation pathway and the product distribution.

CO is the primary product over $Rh/SiO_2$ catalysts after the change from He to $CH_4/O_2/Ar$ was made at 700 °C for the transient reaction (Fig. 5c and 5d) and only a very tiny amount of $CO_2$ was detected. $CO_2$ is the primary product for both preoxidized and prereduced $Ru/SiO_2$ catalysts at 500 and 700 °C, implying that the concentration of oxygen species on the catalyst may have a significant influence on the reaction schemes for POM. Based on TAP (temporal analysis of products) studies of POM over individual metal or supported metal catalysts, such as Rh sponge [52], $Rh/Al_2O_3$ [52,53], and Pt gauze [32], some researchers have concluded that the formation of primary products depends on the amount/concentration of oxygen species on the catalyst surface. This suggests that the amount of oxygen on $Rh/SiO_2$ surfaces where direct oxidation of methane to syngas occurs will be less than that on $Ru/SiO_2$ surfaces where the POM occurs via an indirect combustion/reforming mechanism.

In situ microprobe Raman spectroscopy characterization of the 4 wt% preoxidized $Rh/SiO_2$ surface exhibited the loss within 2 min of the broad 491 $cm^{-1}$ band of $Rh_2O_3$ (found at 500 °C under $O_2$) [42], when the gas flow was switched to $H_2$/Ar at 500 °C. The Raman spectrum of this catalyst recorded under a simulated POM feed ($CH_4/O_2/Ar$ = 2/1/45) is very similar to that recorded under the $H_2$/Ar atmosphere. No $Rh_2O_3$ was detected. Similar spectra were obtained when heating the catalyst in a $CH_4/O_2/Ar$ between 500 and 600 °C. Clearly, most of the Rh species over the $Rh/SiO_2$ are in the metallic state during POM. Mallens et al. [32] reached the same conclusion from their TAP experiment, where by assuming the $Rh_2O_3$ oxide stoichiometry, only 0.4 wt% of $Rh_2O_3$ is present during the simultaneous interaction of $CH_4$ and $O_2$ at a stoichiometric feed ratio ($CH_4/O_2 = 2/1$) over the rhodium sponge.

Raman bands (489 and 609 $cm^{-1}$) attributed to $RuO_2$ [46,47] were observed for the 4 wt% $Ru/SiO_2$ under $O_2$ at 500 to 600 °C. These bands disappeared when the preoxidized 4 wt% $Ru/SiO_2$ was exposed to $H_2$/Ar at 500 to 600 °C and reappeared when the $H_2$/Ar pretreated $Ru/SiO_2$ was switched to a flow of $CH_4/O_2/Ar$ at the same temperature. Thus, the Ru species of the $Ru/SiO_2$ catalyst are almost fully oxidized under the POM conditions. In situ microprobe Raman characterizations of $Rh/SiO_2$ and $Ru/SiO_2$ catalyst (Fig. 6) under POM conditions correspond to pulse and transient reaction results, showing that a significant difference in mechanism exists over these two catalysts. The concentration of oxygen species on the catalyst surface causes the mechanistic change. No Raman band of $Rh_2O_3$ species was detected in a working-state $Rh/SiO_2$. Even at the top of the catalyst bed, most of the Rh is in the metallic state during POM. $CH_4$ is activated and dissociated to $CH_x$ ($x = 0$–3)

species on $Rh^0$ sites and then converted to CO through surface reactions, such as H dissociation from $CH_x$ and the oxidation of surface C or $CH_x$ ($x = 1$–3) species by surface oxygen species (e.g., $O^{2-}$).

In contrast to $Rh/SiO_2$, the Ru species on $Ru/SiO_2$ near the entrance of the catalyst bed are almost fully oxidized under the reaction conditions. Transient and pulse reactions show that oxidized Ru species catalyze the complete oxidation of $CH_4$ to $CO_2$, causing complete oxygen consumption from the feed ($CH_4/O_2$) within a narrow zone at the entrance of the catalyst bed. Ru located in the rest of catalyst bed is reduced by the $CH_4$ remaining in the feed to the metallic state. Reforming of the resulting $CH_4/CO_2/H_2O$ to syngas occurs at such reduced Ru sites. The oxygen species on the catalysts could be surface $O^{2-}$. Surface $O^{2-}$ is responsible for both the selective and complete oxidation of methane, depending on its concentration. The significant catalytic differences of $Rh/SiO_2$ and $Ru/SiO_2$ may be related to the large differences in the Rh–O (405.0 kJ/mol) and Ru–O (528.4 kJ/mol) bond strengths [54]. This renders the reduction of $Ru/SiO_2$ more difficult than that for $Rh/SiO_2$. For example, temperature-programmed reductions (Fig. 2) demonstrate a lower reduction temperature for 1 wt% $Rh/SiO_2$ relative to 1 wt% $Ru/SiO_2$. The $Ru(O)/SiO_2$ surface chemistry differs from that of $Rh(O)/SiO_2$. $O_2$ dissociates to form Ru–O species on metallic Ru sites, eventually generating a $RuO_2$ surface phase that is not easily decomposed. $RuO_2$ inhibits C–H dissociation, desorption of $CH_x$, and reaction of $CH_x$ fragments with dissociatively adsorbed oxygen. The high surface $RuO_2$ concentration on $Ru/SiO_2$ during low-temperature (450–600 °C) POM contrasts sharply with the surface composition of $Rh/SiO_2$. $CH_4$ cannot dissociate over metallic ruthenium sites and so cannot react via a direct surface oxidation process. However, $CH_4$ can be oxidized via a nonselective indirect mechanism [55] ($CH_4 + 2RuO_2 \rightarrow CO_2 + 2H_2O + 2Ru^0$) where $CO_2$ is a primary product over the ruthenium catalyst. Therefore, POM over $Ru/SiO_2$ occurs mainly via an indirect nonselective oxidation process. The selectivity of $Ru/SiO_2$ is lower than that of $Rh/SiO_2$.

The low Rh–O bond strength leads to a much lower surface oxygen coverage on $Rh/SiO_2$ catalyst during POM. Surface oxygen on oxidized $Rh(O)/SiO_2$ begins to thermally desorbed at 550 °C according to the $O_2$-TPD experiments (Fig. 3). Reduction of rhodium oxides started at 80 °C and peaked at 120 °C in TPR experiments, so the $Rh/SiO_2$ surface must be metallic Rh during POM since $H_2$ is present. Consequently, partial oxidation of $CH_4$ to syngas over $Rh/SiO_2$ proceeds mainly via a direct oxidation [56,57], in which $CH_4$ and $O_2$ react at the metal surface via their dissociated and adsorbed species.

The gas hourly space velocity (GHSV) $CH_4/O_2 = 2/1$ (Table 2) has little effect on the performance of $Rh/SiO_2$ at 500 °C when increased from 100,000 to 150,000 $h^{-1}$. The $CH_4$ conversion and selectivities to $H_2$ and CO decreased slightly, $CH_4$ conversion from 68.8 to 67.0%, CO selectivity from 59.1 to 56.5%, and $H_2$ selectivity from 69.5 to 66.2%. A more significant effect on $Ru/SiO_2$ occurred when GHSV increased from 100,000 to 150,000 $h^{-1}$. Methane conversion decreased from 66.3 to 61.1%; CO selectivity dropped from 57.9 to 45.4%, and $H_2$ selectivity reduced from 66.5 to 53.6%. These results also support direct oxidation with $Rh/SiO_2$ and indirect combustion/reforming over $Ru/SiO_2$, in agreement with POM mechanisms proposed based on the in situ micro-Raman, pulse and transient reactions studies.

### 4.2. Primary product determination by transient reactions

A main concern in the POM mechanism debate is whether $CO_2$ or CO is the primary product. For the direct oxidation scheme, CO is the primary product whereas $CO_2$ should be formed prior to CO in the indirect process. The TAP reactor has been used to monitor CO and $CO_2$ formation during the POM reaction [25,32–34,37,38,52,53,58,59]. Responses to pulses of $O_2$, $CH_4$, or $CH_4/O_2$ over catalysts under different conditions have provided mechanistic information. Most TAP studies focused on the POM over platinum and rhodium. No TAP study of POM with a ruthenium catalyst has been reported, although Ru supported on $TiO_2$ is an effective catalyst for POM via a direct route [22,31,60,61]. Mechanistic results from TAP studies of a similar catalyst still do not agree about the primary reaction products [32,38]. Weng et al. [39,40] used in situ TR-FTIR spectroscopy to follow the primary products over $SiO_2$-supported rhodium and ruthenium catalysts from 500 to 600 °C. CO was the primary POM product over hydrogen-reduced and working-state Rh catalysts. In contrast, $CO_2$ was the primary POM product over supported Ru catalysts. Therefore, direct oxidation of $CH_4$ was proposed with $Rh/SiO_2$, while the reforming of unreacted $CH_4$ to syngas dominated using $Ru/SiO_2$. This was accompanied by oxidation of a portion of the $CH_4$ to $CO_2$ and $H_2O$.

Transient reactions (Fig. 5) were used in the current study to determine the primary POM products over $SiO_2$-supported rhodium and ruthenium catalysts at temperatures at 500 and 700 °C. When $O_2$-pretreated 1 wt% $Rh/SiO_2$ was subjected to a step change from helium to $CH_4/O_2/Ar$ (2/1/45) at 700 °C, CO appeared before $CO_2$ (Fig. 5c). Similar results were obtained for prereduced $Rh/SiO_2$ (Fig. 5d). These results agree with the TAP study of POM at 600 °C over unsupported Pt and Rh catalysts by Mallens et al. [32,33] where direct oxidation of $CH_4$ occurred upon pulsing with $O_2$, $CH_4$, or $CH_4/O_2$. At comparable temperatures, the Rh catalyst shows a higher methane conversion and greater selectivity to both CO and $H_2$ than Pt. Fathi et al. [34] also showed that POM could be attributed to a direct mechanism using a TAP-2 reactor over Pt gauze at temperatures above 800 °C. In this current study, transient reactions prove that $CO_2$ is the primary POM product over both preoxidized and prereduced 1 wt% $Ru/SiO_2$ at 500 and 700 °C. CO is only detected after $CO_2$. CO results from combustion of $CH_4$ to $CO_2$ and $H_2O$, followed by reforming. Buyevskaya et al. [25,38], Guerrero-Ruiz et al. [62], and

Boucouvalas et al. [63] came to a similar conclusion about POM based on in situ diffuse reflectance infrared Fourier transform spectroscopy (DRIFTS), kinetics, and isotopic tracing and TAP reactor studies.

## 5. Conclusions

Methane conversion and selectivity to both $H_2$ and CO were higher over $Rh/SiO_2$ than $Ru/SiO_2$. The CO and $H_2$ selectivities substantially decreased with increasing GHSV over $Ru/SiO_2$ at 500 °C but remained nearly constant over $Rh/SiO_2$. Both the $CH_4$ conversions and the CO and $H_2$ selectivities increased slightly over both catalysts at 700 °C as GHSV increases, while the $CH_4$ conversions and the CO and $H_2$ selectivities decreased slightly. CO was the main product at 700 °C when $Rh/SiO_2$ was exposed to methane pulses, whether the catalyst was preoxidized or prereduced. $CO_2$ was only detected during the first pulse over $Rh/SiO_2$ catalyst. More $CO_2$ was formed over $Ru/SiO_2$ than $Rh/SiO_2$ during the first pulse; $CO_2$ was formed at every pulse over $Ru/SiO_2$.

CO formed before $CO_2$ over preoxidized or prereduced $Rh/SiO_2$ at 700 °C in transient reactions, induced by changing the feed gas from helium to $CH_4/O_2/Ar$. $CO_2$ is the primary product over $Ru/SiO_2$ catalysts during transient reactions.

In situ microprobe Raman spectroscopy demonstrated that the oxide levels present on $Ru/SiO_2$ were far higher during POM than those on $Rh/SiO_2$. The mechanisms of POM over these two catalysts are different. On the $Rh/SiO_2$ catalyst, POM is mainly a direct oxidation process, while on the $Ru/SiO_2$ catalyst, the dominant pathway of POM is the indirect oxidation process.

## Acknowledgments

This project is generously supported by the Ministry of Science and Technology of China (No. G1999022408), National Natural Science Foundation of China (Nos. 20023001, 2002100), the Center for Advanced Vehicular Systems (CAVS), and the support from the National Science Foundation (EPS0132618) and the US Environmental Protection Agency (USMGR0129001) are gratefully acknowledged.

## References

[1] J.M. King, M.J. O'Day, J. Power Sources 86 (1–2) (2000) 16.
[2] M.R. Gardiner, J. Cunningham, R.M. Moore, Fuel Cells and Alternative Fuels/Energy Systems, Society of Automotive Engineers, 2001, [Special publication] SP-1635, p. 65.
[3] D.P. Wilkinson, Electrochem. Soc. Interface 10 (1) (2001) 22.
[4] S.C. Amendola, S.L. Sharp-Goldman, M.S. Janjua, N.C. Spencer, M.T. Kelly, P.J. Petillo, M. Binder, Int. J. Hydrogen Energy 25 (10) (2000) 969.
[5] J.P. Van Hook, Catal. Rev.-Sci. Eng. 21 (1981) 1.
[6] M. Prettre, Ch. Eichner, M. Perrin, Trans. Faraday Soc. 43 (1946) 335.
[7] A.T. Ashcroft, A.K. Cheetham, J.S. Foord, M.L.H. Green, C.P. Grey, A.J. Murrel, P.D.F. Veron, Nature 344 (1990) 319.
[8] V.A. Tsipouriari, Z. Zhang, X.E. Verykios, J. Catal. 179 (1998) 283.
[9] C.T. Au, H.Y. Wang, J. Catal. 167 (1997) 337.
[10] D. Dissanayake, M.P. Rosynek, K.C.C. Kharas, J.H. Lunsford, J. Catal. 132 (1991) 117.
[11] E. Ruckenstein, Y.H. Hu, Ind. Eng. Chem. Res. 37 (1998) 1744.
[12] R. Drago, S. Jurczyk, K. Kob, N. Bhattacharyya, A. Masin, J. Catal. Lett. 51 (1998) 177.
[13] Q. Yan, Z. Chao, T. Wu, W. Weng, H. Wan, Stud. Surf. Sci. Catal. 130D (2000) 3549.
[14] K. Nakagawa, N. Ikenaga, Y. Teng, T. Kobayashi, T. Suzuki, J. Catal. 186 (1999) 405.
[15] H.D. Gesser, N.R. Hunter, Catal. Today 42 (3) (1998) 183.
[16] C. Mirodatos, Stud. Surf. Sci. Catal. 119 (1998) 99.
[17] D.A. Hickman, L.D. Schmidt, AIChE J. 39 (1993) 1164.
[18] D.A. Hickman, L.D. Schmidt, Science 259 (1993) 343.
[19] D.A. Hickman, L.D. Schmidt, J. Catal. 136 (2) (1992) 300.
[20] D.A. Hickman, L.D. Schmidt, J. Catal. 138 (1) (1992) 267.
[21] L.D. Schmidt, M. Huff, S.S. Bharadwaj, Chem. Eng. Sci. 49 (24A) (1994) 3981.
[22] Y. Boucouvalas, Z.L. Zhang, X.E. Verykios, E. Xenophon, Catal. Lett. 40 (3,4) (1996) 189.
[23] L.D. Schmidt, M. Huff, S.S. Bharadwaj, Chem. Eng. Sci. 49 (24A) (1994) 3981.
[24] M.C.J. Bradford, M.A. Vannice, Catal. Today 50 (1999) 87.
[25] O.V. Buyevskaya, D. Wolf, M. Baerns, Catal. Lett. 29 (1994) 249.
[26] P.M. Witt, L.D. Schmidt, J. Catal. 163 (1996) 465.
[27] P.M. Torniainen, X. Chu, L.D. Schmidt, J. Catal. 146 (1994) 1.
[28] W.J.M. Vermeiren, E. Blomsma, P.A. Jacobs, Catal. Today 13 (1992) 427.
[29] D. Dissanayake, M.P. Rosynek, J.H. Lunsford, J. Phys. Chem. 97 (1993) 3644.
[30] V.R. Choudhary, A.M. Rajput, B. Prabhakar, J. Catal. 139 (1993) 326.
[31] C. Elmasides, X.E. Verykios, J. Catal. 203 (2) (2001) 477.
[32] J.E.P. Mallens, J.H.B.J. Hoebink, G.B. Marin, J. Catal. 167 (1997) 43.
[33] E.P.J. Mallens, J.H.B.J. Hoebink, G.B. Marin, Catal. Lett. 33 (1995) 291.
[34] M. Fathi, F. Monnet, Y. Schuurman, A. Holmen, C. Mirodatos, J. Catal. 190 (2000) 439.
[35] D. Qin, J. Lapszewicz, X. Jiang, J. Catal. 159 (1996) 140.
[36] C. Li, C. Yu, S. Shen, Catal. Lett. 67 (2–4) (2000) 139.
[37] K. Walter, O.V. Buyevskaya, D. Wolf, M. Baerns, Catal. Lett. 29 (1,2) (1994) 261.
[38] O.V. Buyevskaya, K. Walter, D. Wolf, M. Baerns, Catal. Lett. 38 (1,2) (1996) 81.
[39] W. Weng, M. Chen, Q. Yan, T. Wu, Z. Chao, Y. Liao, H. Wan, Catal. Today 63 (2000) 317.
[40] W. Weng, Q. Yan, C. Lou, Y. Liao, et al., Stud. Surf. Sci. Catal. 136 (2001) 233.
[41] C. Hoang-van, Y. Kachaya, S.J. Teichner, J.A. Dalmon, Appl. Catal. 46 (1989) 81.
[42] C.T. Williams, C.G. Takoudis, M.J. Weaver, J. Phys. Chem. B 102 (1998) 406.
[43] L. Ji, J. Lin, H.C. Zeng, Chem. Mater. 13 (7) (2001) 2403.
[44] N.N. Greenwood, A. Earnshaw, Chemistry of the Elements, Pergamon, Oxford, 1984, p. 1297.
[45] D.D. Beck, T.W. Capehart, C. Wong, D.N. Belton, J. Catal. 144 (1993) 311.
[46] S.Y. Mar, C.S. Chen, Y.S. Huang, K.K. Tiong, Appl. Surf. Sci. 90 (1995) 497.
[47] Y.S. Huang, P.C. Liao, Sol. Energy Mater. Sol. Cells 55 (1998) 179.
[48] D.R. Lide (Ed.), CRC Handbook of Chemistry and Physics, seventy-eighth ed., Chemical Rubber Company Press, Boca Raton, FL, 1997, pp. 4–50.

[49] A. Frydman, D.G. Castner, M. Schmal, C.T. Campbell, J. Catal. 152 (1995) 164.
[50] J. Emsley, The Elements, second ed., Clarendon, Oxford, 1991, p. 172.
[51] V.I. Parvulescu, S. Coman, P. Palade, D. Macovei, C.M. Teodorescu, G. Filoti, R. Molina, G. Poncelet, F.E. Wagner, Appl. Surf. Sci. 141 (1999) 164.
[52] H.K. Hofstad, J.H.B.J. Hoebink, A. Holmen, G.B. Marin, Catal. Today 40 (1998) 157.
[53] D. Wang, O. Dewaele, A.M. De Groote, G.F. Froment, J. Catal. 159 (1996) 418.
[54] J.B. Pedley, E.M. Marshall, J. Phys. Chem. Ref. Data 12 (1984) 967.
[55] H.Y. Wang, E. Ruckenstein, J. Catal. 186 (1999) 181.
[56] Y.H. Hu, E. Ruckenstein, J. Phys. Chem. A 102 (1998) 10,568.
[57] Y.H. Hu, E. Ruckenstein, J. Phys. Chem. B 102 (1998) 230.
[58] M. Soick, O. Buyevskaya, M. Höhenberger, D. Wolf, Catal. Today 32 (1996) 163.
[59] M. Soick, D. Wolf, M. Bearn, Chem. Eng. Sci. 55 (2000) 2875.
[60] Y. Boucouvalas, Z.L. Zhang, A.M. Efstathiou, X.E. Verykios, Stud. Surf. Sci. Catal. 101 (1996) 443.
[61] C. Elmasides, D.I. Kondarides, W. Grünert, X.E. Verykios, J. Phys. Chem. 103 (1999) 5227.
[62] A. Guerrero-Ruiz, P. Ferreira-Aparicio, M.B. Bachiller-Baeza, I. Rodríguez-Ramos, Catal. Today 46 (1998) 99.
[63] Y. Boucouvalas, Z.L. Zhang, X.E. Verykios, Catal. Lett. 27 (1994) 131.